Supporting information

$CoSe/CoSe_2$ Mott–Schottky heterostructures embedded in porous carbon nanofibers toward efficient bifunctional catalysis in zinc–air batteries

Yang Song,[a,§] Depeng Zhang, [a,§] Yuqing Zhang,[a] and Chao Deng[a,*]

[a]Key Laboratory for Photonic and Electronic Bandgap Materials, Ministry of Education; College of Physics and Electric Engineering, Harbin Normal University, Harbin, 150025, Heilongjiang, China

* Corresponding author

E-Mail: chaodenghsd@126.com (C. Deng)

§ Both authors contribute equally to this work

Part I: Experimental details, Calculations & Discussions

S-1: Preparation of the samples

S-1-1: Preparation of $CoSe/CoSe_2$@PNC

i) Preparation of the precursor by electrospinning

The single-nozzle was used in the electrospinning to prepare the precursor. The 0.8 g polyvinylpyrrolidone (PVP, MW 1300000, Aladdin, China), 6ml polytetrafluoroethylene (PTFE, Songbaihuagong, China), and 0.35 g cobalt acetate tetrahydrate (AR, 99.5%, Macklin, China) were dissolved in 2 ml deionized water (DI water), and stirred for 6 h to obtain a uniform solution. Subsequently, this homogeneous solution was injected into the syringe and ensured that the syringe was tightly connected to the single-nozzle channel of the electrospinning machine. The positive and negative voltages were regulated to ~20 kV and the distance between the needle and the collector was ~25 cm. After the electrospinning process, the film was peeled off from the collector, and the precursor was achieved.

ii) Preparation of the intermediate product for Co@PNC

The electrospinning precursor was initially stabilized in the air at 230 °C for 2 hours. Subsequently, the product was kept at 700 °C under an inert atmosphere for 3 hours, then cooled naturally to room temperature to obtain the Co@PNC.

iii) Preparation of the $CoSe/CoSe_2$@PNC

The intermediate products Co@PNC and selenium powder (99.99%, Macklin, China) were placed downstream and upstream of the quartz tube, respectively, and heated up to 450 °C at a heating rate of 3 °C/min under an N_2 atmosphere and kept for 3 h. After cooling to room temperature, $CoSe/CoSe_2$@PNC was obtained.

S-1-2: Preparation of the reference samples

i) Preparation of the CoSe@PNC

The preparation of the CoSe@PNC standard samples follows the same procedure as for CoSe/$CoSe_2$@PNC, with the exception that the amount of selenium powder used is reduced by half.

ii) Preparation of the $CoSe_2$@PNC

The preparation of the $CoSe_2$@PNC standard samples follows the same procedure as for CoSe/$CoSe_2$@PNC, with the exception that the amount of selenium powder used is increased to 3 times the original quantity.

S-2: Materials characterizations

Powder X-ray diffraction (XRD, Bruker D8/Germany) using Cu Kα radiation was employed to identify the crystalline phase of the material. The morphology was observed with a scanning electron microscope (SEM, HITACHIS-4700) and a transmission electron microscope (TEM, JEOS-2010 PHILIPS). X-ray photoelectron spectroscopy (XPS, Thermo ESCALAB 250) was employed to measure the chemical or electronic state of each element. Raman spectra were collected on a (J-Y T6400) Raman spectrometer with 514.5 nm wavelength incident laser light. Work function was measured by ultraviolet photoelectron spectroscopy (UPS, Thermo Fisher ESCALAB Xi+). Nitrogen adsorption-desorption isotherms were measured using a Micromeritics ASAP 2010. s

S-3: Electrochemical measurements on electrocatalysis

S-3-1 Evaluation of the ORR/OER catalytic properties

The electrochemical measurements were conducted on a rotating electrode system (Pine Inc.) with a CHI electrochemical workstation. A three-electrode system was used with a glassy carbon rotating disk electrode (5 mm in diameter) with fixed hollow fibers as the working electrode, a graphitic rod as the counter electrode, and a Hg/HgO electrode as the reference electrode. The KOH solution was used as the

electrolyte. All the potentials were transferred into the reversible hydrogen electrode (RHE) form according to the Nernst equation.

$E_{RHE} = E_{Hg/HgO} + 0.059 \times pH + 0.098\ V$ (1)

The pure oxygen was purged in the electrolyte for 20~30 minutes before the tests. Before cyclic voltammetry (CV) and linear sweep voltammetry (LSV) measurements, the working electrodes were activated by CV tests. Linear sweep voltammetry (LSV) for ORR polarization curves was conducted at rotating speeds of 1600 rpm.

S-4 Fabrication and evaluation of Zn-air battery

S-4-1 Fabrication of aqueous Zn-air battery

The Zn-air battery was performed in a home-built electrochemical cell. The polished commercial Zn foil was used as the anode and a piece of Co/CoSe@MNCF film as the air cathode. Meanwhile, KOH electrolyte with $Zn(CH_3COO)_2$ was used as electrolyte. All the measurements were conducted on the as-constructed cell at room temperature with the CHI electrochemical workstation and LAND battery testing system (Wuhan, China). The specific capacities are calculated from the galvanostatic discharge results, normalized to the mass of consumed Zn.

S-4-2 Fabrication of flexible Zn-air battery

i) Preparation of the polymer gel electrolyte

The hydrogel electrolyte was prepared according to the process reported in previous reports [S1]. Firstly, the concentrated sodium hydroxide solution was slowly dropped into an aqueous solution of acrylic acid monomer with continuously stirring in ice-bath. Next, the initiator of ammonium persulphate and crosslinker of N, N'-methylene diacrylamide were added to the mixed solution. After magnetic stirring for thirty minutes, the solution was degassed to remove the dissolved oxygen and sealed under N_2. Then the free-radical polymerization was initiated to proceed at 65 ^oC. After that,

the product was peeled off and dried in an oven. Then the resultant product was fully soaking in the mixed electrolyte of potassium hydroxide to achieve the equilibrate state. Finally, the polymers were wipe-dried with paper tissues and the obtained polymer hydrogels was used as quasi-solid-state electrolytes.

ii)Preparation of the carbon matrix@Zn anode

The carbon matrix@Zn anode was prepared according to the process reported in previous reports [S2,S3]. Firstly, the carbon matrix was prepared by an electrospinning process and the following calcinations. The polyvinyl pyrrolidone (PVP, Macklin, China), polytetrafluoroethylene (PTFE, 3M, USA), and copper acetate hydrate (Macklin, China) were dissolved in distilled water to achieve a transport solution. Then the electrospinning solution was loaded into the syringe under a high voltage of 18~21 kV. After the electrospinning process, the film was peeled off from the collector, and the precursor was achieved. The prepared precursor was firstly stabilized at 230 ^{o}C in air; Then it was calcinated at 800 ^{o}C for 2 h with the heating rate of 2 ^{o}C min^{-1} in a nitrogen atmosphere to achieve the carbon matrix host. Next, the Zn electrodeposition was carried out. The Zn foil and glass fiber were used as the counter/reference electrode and separator, respectively. The aqueous $ZnSO_4$ (2 mol L^{-1}) and H_3BO_3 solution was used as the electrolyte. The electrodeposition was conducted at room temperature. Then the carbon matrix@Zn electrode was washed with DI water and dried in a vacuum oven at 60 ^{o}C.

iii) Fabrication of flexible Zn-air battery

The flexible ZAB was prepared by using the $CoSe/CoSe_2$@PNC cathode, the carbon matrix@Zn anode and the polymer hydrogel electrolyte. The sandwich group was packed with the cathode surface exposure, and result in the flexible Zn-air battery.

The galvanostatic charge/discharge tests were conducted on a LAND battery testing system (Wuhan, China).

S-5 Density functional theory (DFT) methods

The theoretical calculations were carried out using the density functional theory and the plane-wave pseudopotential method [S4,S5]. The generalized gradient approximation (GGA) of Perdew-Burke-Ernzerhof (PBE) exchange correlation function [S6,S7] was adopted. All geometric optimizations and energy calculations were performed using periodic boundary conditions with adjacent adsorbents and adsorbents to prevent configurational interactions.

Part II: Supporting Figures

Figure S1

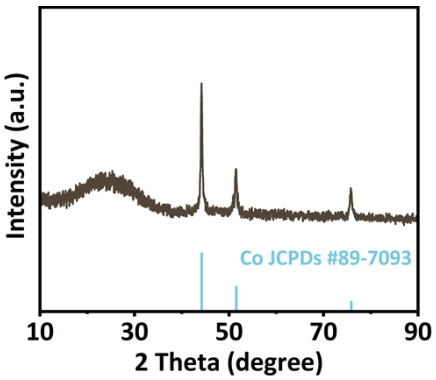

Figure S1 XRD pattern of Co@PNC fiber.

Figure S2

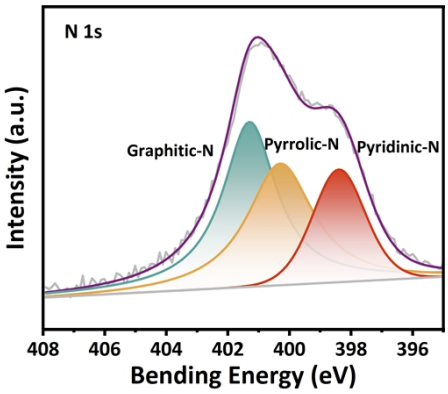

Figure S2 N 1s XPS spectra of Co@PNC fiber.

Figure S3

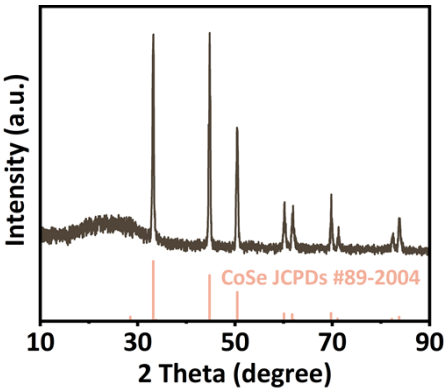

Figure S3 XRD pattern of the CoSe@PNC reference sample.

Figure S4

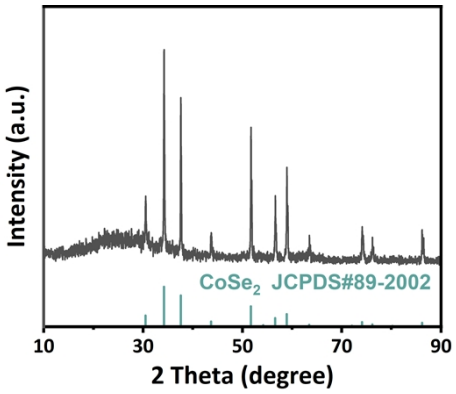

Figure S4 XRD pattern of the $CoSe_2$@PNC reference sample.

Figure S5

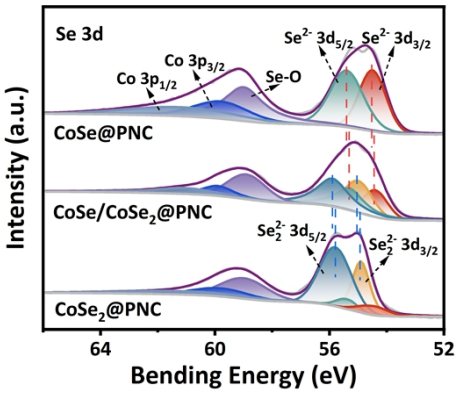

Figure S5 Comparison of Se 3d XPS spectra of CoSe/$CoSe_2$@PNC, $CoSe_2$@PNC and CoSe@PNC.

Figure S6

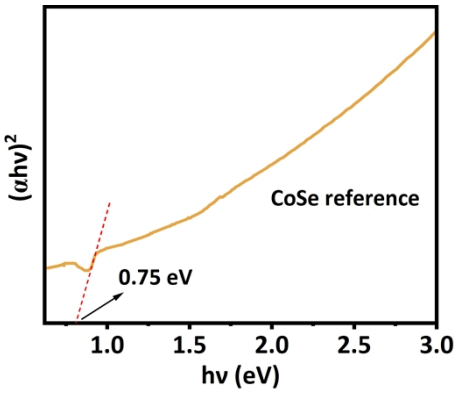

Figure S6 UV-Vis-NIR of the CoSe reference.

Figure S7

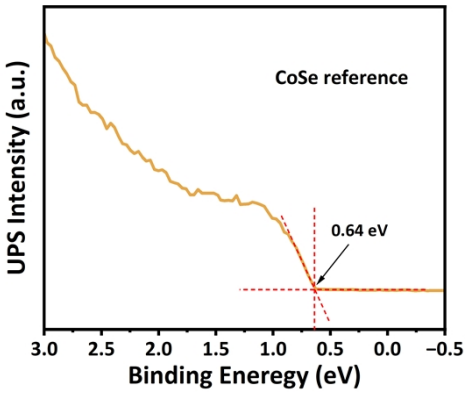

Figure S7 UPS spectra of the CoSe reference around Femi energy level.

Figure S8

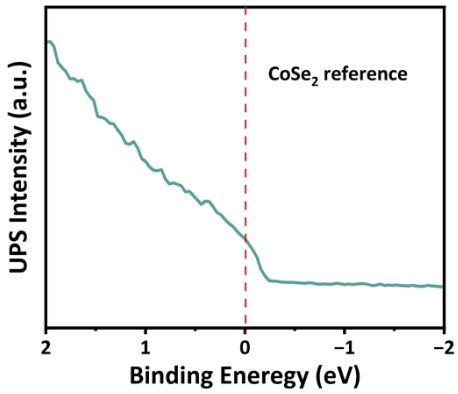

Figure S8 UPS spectra of the $CoSe_2$ reference around Femi energy level.

Figure S9

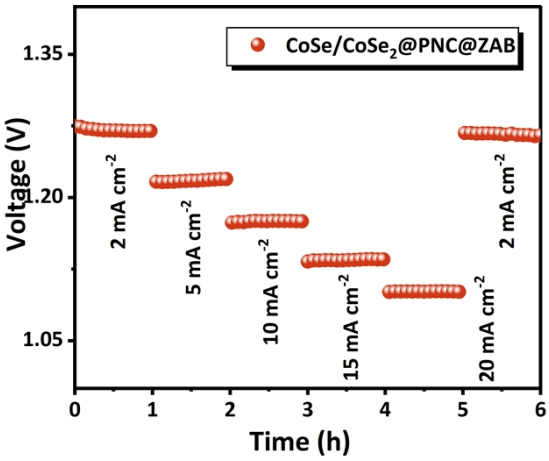

Figure S9 Discharge curves of the CoSe/$CoSe_2$@PNC@ZAB at various current densities.

Part III: Supporting Tables

Table S1 Performance comparison of $CoSe/CoSe_2$@PNC and the reference catalysts in previous reports

Materials	$E_{1/2}$/V	Tafel Slope for ORR (mV dec^{-1})	$E_{j=10}$/mV	Tafel Slope for OER (mV dec^{-1})	ΔE/V	References
Co-NC/$CoFe_2O_4$	0.81	74.32	270	83.3	0.690	[S8]
$CoMoO_4$@NC-Co	0.83	93.2	322	64	0.722	[S9]
$MnCo_2O_4/Mn_2O_3$ NR	0.83	99	332	51	0.732	[S10]
CoFe@NC-5	0.84	66	367	57.77	0.757	[S11]
Co/$CoSe_2$@NSeC	0.789	43.38	340	76.74	0.781	[S12]
CNC/Co_9S_8@SNCF	0.87	73	359	88	0.719	[S13]
P-Co/CoOV@ NHCNB@NCNT	0.855	62.49	377	159.12	0.752	[S14]
$CoSe/CoSe_2$@PNC	0.836	62.79	316	65.06	0.710	This work

Part IV: Supporting References

[S1] Z.X. Pei, Z.W. Yuan, C.J. Wang, S.L. Zhao, J.Y. Fei, L. Wei, J.S. Chen, C. Wang, R.J. Qi, Z.W. Liu, Y. Chen, A flexible rechargeable zinc-air battery with excellent low-temperature adaptability, Angew. Chem. Int. Ed. 59 (2020) 4793–4799. https://doi.org/10.1002/ange.201915836.

[S2] Y.X. Zeng, P.X. Sun, Z.H. Pei, Q. Jin, X.T. Zhang, L. Yu, X. Lou, Nitrogen-doped carbon fibers embedded with zincophilic Cu nanoboxes for stable Zn-metal anodes, Adv. Mater. 34 (2022) 2200342. https://doi.org/10.1002/adma.202200342.

[S3] Y.K. Liu, B. Li, J. Wang, C.y Li, H.R. Yang, Y. Song, S. Zhang and C. Deng, Asymmetric Zn-N_4 atomic sites embedded hollow fibers as stable Zn anode for high-performance Zn-ion hybrid capacitor, J. Energy Chem. 97 (2024) 460–469. https://doi.org/10.1016/j.jechem.2024.06.006.

[S4] G. Kresse, J. Furthmüller, Efficient iterative schemes for ab initio total-energy calculations using a plane-wave basis set, Phys. Rev. B 54 (1996) 11169–11186. https://doi.org/10.1103/physrevb.54.11169.

[S5] G. Kresse, J. Hafner, Ab initio molecular-dynamics simulation of the liquid-metal-amorphous-semiconductor transition in germanium, Phys. Rev. B 49 (1994) 14251–14269. https://doi.org/10.1103/physrevb.49.14251.

[S6] J. Wang, J. Polleux, J. Lim, B. Dunn, Pseudocapacitive contributions to electrochemical energy storage in TiO_2 (anatase) nanoparticles, J. Phys. Chem. C 111 (2007) 14925–14931. https://doi.org/10.1021/JP074464W.

[S7] P.E. Blöchl, Projector augmented-wave method, Phys. Rev. B 50 (1994) 17953–17979. https://doi.org/10.1103/physrevb.50.17953.

[S8] L.M. Yang, T. Yang, J.H. Liu, S.B. Dong, S. Liu, K. Wang, E.H. Wang, H.Y. Wang, K.C. Chou, X.M. Hou, Regulating local charge distribution via schottky

heterojunctions for ultra-stable zinc-air batteries, Acta Mater. 303 (2026) 121718. https://doi.org/10.1016/j.actamat.2025.121718.

[S9] Q.W. Feng, H.C. Kang, Y. Xiao, B.T. Su, Z.Q. Lei, Bifunctionality of $CoMoO_4$ nanorods with Co, N co-doped carbon heterostructures can be used in zinc-air batteries, J. Energy Storage 122 (2025) 116740. https://doi.org/10.1016/j.est.2025.116740.

[S10] R.R. Ayyaluri, B.N.V. Krishna, O.R. Ankinapalli, Y.J. Lee, L. Natarajan, J.S. Yu, $MnCo_2O_4/Mn_2O_3$ nanorod architectures as bifunctional electrocatalyst material for rechargeable zinc-air batteries, ACS Sustainable Chem. Eng. 12 (2024) 10765–10775. https://doi.org/10.1021/acssuschemeng.4c01477.

[S11] X.W. Song, M. Lin, H. Zhao, R.X. Sun, Y.B. Guan, Heterostructured CoFe/Co nanoalloys encapsulated in N-doped carbon as bifunctional oxygen-electrode catalysts for Zn-air batteries, Phys. Chem. Chem. Phys. 27 (2025) 14504–14516. https://doi.org/10.1039/d5cp00941c.

[S12] H. Seong, K. Min, G. Lee, K. Kwon, S.H. Baeck, Development of an efficient bifunctional electrocatalyst based on $Co/CoSe_2$ nanoparticles embedded in N, Se co-doped carbon for AEMFC and rechargeable Zn-air battery, Appl. Catal. B: Environ. 362 (2025) 124725. https://doi.org/10.1016/j.apcatb.2024.124725.

[S13] C. Yang, J. Chen, L. Yan, Y.J. Gao, J.Q. Ning, Y. Hu, Customizing oxygen electrocatalytic microenvironment with S, N codoped carbon nanofibers confining carbon nanocapsules and Co_9S_8 nanoparticles for rechargeable Zn-air batteries, Appl. Catal. B: Environ. 352 (2024) 124060. https://doi.org/10.1016/j.apcatb.2024.124060.

[S14] L.J. Ye, W.H. Chen, Z.J. Jiang, Z.Q. Jiang, Co/CoO heterojunction rich in oxygen vacancies introduced by O_2 plasma embedded in mesoporous walls of carbon nanoboxes covered with carbon nanotubes for rechargeable zinc-air battery, Carbon

Energy 6 (2024) e457. https://doi.org/10.1002/cey2.457.